Received 19 May 2022; revised 24 July 2022; accepted 3 August 2022. Date of publication 17 August 2022; date of current version 14 October 2022.
The review of this article was arranged by Editor M. Saitoh.

Digital Object Identifier 10.1109/JEDS.2022.3199205

Temperature Driven Current–Voltage Characteristics of Ionic Liquid Type Intelligent Connection Device

MASAKAZU KOBAYASHI[1] (Member, IEEE), YASUMITSU ORII[1] (Senior Member, IEEE), HISASHI SHIMA[2], YASUHISA NAITOH[2], HIROYUKI AKINAGA[2] (Member, IEEE), DAN SATO[3], TAKUMA MATSUO[3], KENTARO KINOSHITA[3], TOSHIKI NOKAMI[4], AND TOSHIYUKI ITOH[5]

1 New Value Creation Office, NAGASE & Company, Ltd., Tokyo 1030024, Japan
2 Device Technology Research Institute, National Institute of Advanced Industrial Science and Technology, Tsukuba 3058565, Ibaraki, Japan
3 Department of Applied Physics, Graduate School of Science, Tokyo University of Science, Tokyo 1258585, Japan
4 Center for Research on Green Sustainable Chemistry, Faculty of Engineering, Tottori University, Tottori 6808552, Japan
5 Toyota Physical and Chemical Research Institute, Aichi 4801118, Japan

CORRESPONDING AUTHORS: M. KOBAYASHI AND H. SHIMA (e-mail: masakazu.kobayashi@nagase.co.jp; shima-hisashi@aist.go.jp)

This work was supported in part by the NIMS Nanofabrication Platform through the Nanotechnology Platform Program of the Ministry of Education, Culture, Sports, Science, and Technology (MEXT), Japan, under Grant JPMXP09F21NM0005.

ABSTRACT The temperature dependence of an intelligent connection (IConnect) device, in which an ionic liquid (IL) plays an essential role in a memristive function is presented in this study. An appropriate choice of IL and dissolved metal ion species can control the volatility of the IL-IConnect device. The temperature dependence of the IL-IConnect device was strong, although the change in current–voltage characteristics was reversible in response to temperature variations. The device's potential as a physical reservoir-computing device is studied.

INDEX TERMS Ionic liquid (IL), intelligent connection (IConnect) device, IL-reservoir device.

I. INTRODUCTION

Development of a novel processing method of artificial intelligent (AI) is a major challenge in advancing the social implementation of AI. Despite the advantage of AI, it requires a significant amount of computational resources. A possible solution to these problems is three-dimensional integration that allows for improved use of devices, interconnects, and subsystems, such as memory and analog-processing circuits, although it is increasingly difficult to control interconnect resistance [1], [2], [3]. A candidate for further technological innovation is to make interconnects intelligent, offering reduced energy loss and high-speed processing. From the heterogeneous integration perspective, a synaptic connection will be created within an intelligent connection (IConnect) device and connecting numerous devices to increase the number of neurons is challenging for packaging technology [4]. Various approaches have been reported for functionalizing the conductive line, notably the IConnect device, formed by conductive chemicals and polymers for information transfer [5], [6], [7], [8], [9], [10], [11]. Conductive bridge random access memory (CBRAM) is a feasible IConnect device owing to its simple structure and low energy consumption. Its electrical properties are similar to those of biological synapses and neurons [12], [13]. An appropriate combination of ionic liquid (IL) and metal ion species added to the IL enables the control of the data volatility of CBRAM [14]. A physical reservoir device with a time–series data treatment function and a high-dimensional feature space is also a feasible candidate of its fading property [15], [16]. Recently, we demonstrated the possibility of using an IL-IConnect device as a physical reservoir [17]. In this study, we developed a simple symmetric separated Pt electrode structure and connected it with supplying of IL in which Cu ion dissolved. We assumed that the key to transmitting input information to the output of the IL-IConnect device would be achieving a smooth electrochemical reaction of metal ions in IL [18], [19], [20]. Furthermore, the electrochemical redox

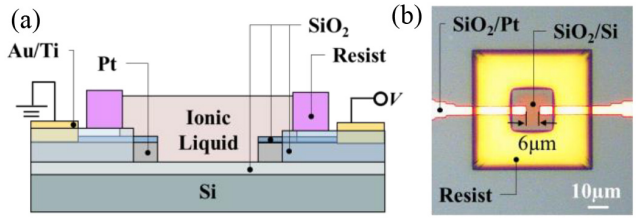

FIGURE 1. (a) Schematic of the device cross-section and (b) optical microscope image of the IL-IConnect device. The gap between the Pt electrode is 6μm.

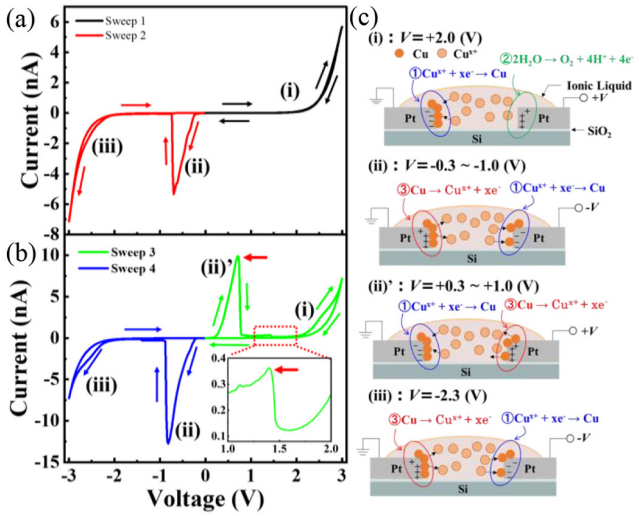

FIGURE 2. I–V curves for (a) first and (b) second cycles measured at room temperature. Red dotted rectangular area was expanded the scale. Two peaks were observed. (c) Schematic images of hypothetical electrochemical reaction occurred at each electrode.

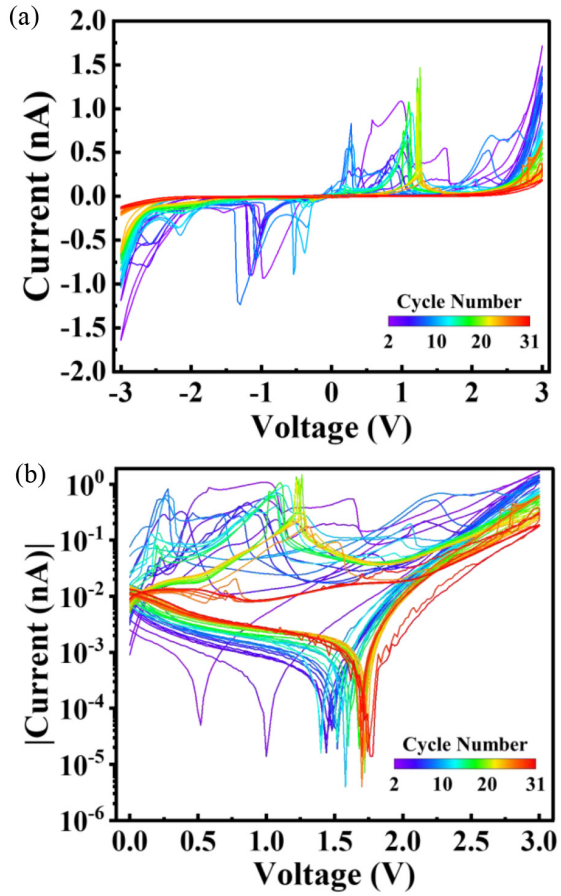

FIGURE 3. (a) Continuous cycle characteristics conducted at a sweep speed of 50 mV/sec and 25°C. (b) Log plot of positive cycle (0V → +3V → 0V) with absolute value of current.

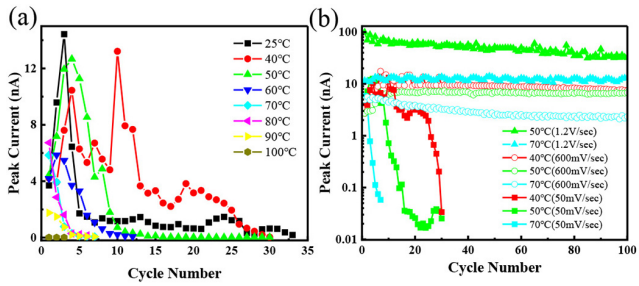

FIGURE 4. (a) Cycle number dependence of the peak current at various temperatures with the sweep rate of 50 mV/sec. (b) Cycle number dependence of the peak current at various temperatures with the sweep rate of 50 mV/sec, 600 mV/sec and 1.2 V/sec.

reaction of Cu ion in the IL follows the Arrhenius equation, which denotes that temperature is a variable factor in the reaction and may be changed to control the redox reaction rate. As a result, we investigated how temperature influences the redox reaction of Faraday current signals in IL-IConnect device [21].

II. DEVICE STRUCTURE AND MEASUREMENT

Ta(1 nm)/Pt(20 nm)/Ta(1 nm) electrode layers were sputtered on a SiO_2/Si substrate and covered with a SiO_2(20 nm) layer that was deposited using the chemical vapor deposition (CVD) method. The top and bottom Ta layers are adhesion layers that ensure adhesion to the upper and lower SiO_2 layers, respectively [22]. The conventional photolithography and dry-etching process were used to microfabricate a planer-type wire-shaped two-terminal structure. Expect for the opposite wire tips, which are a reactive area required for the device operation, the sidewall of the wire-shaped device was coated with CVD-SiO_2(20 nm). Au(100 nm)/Ti(10 nm) contact pads were prepared using the liftoff process after removing the CVD-based SiO_2 layer with buffered hydrofluoric acid. To prevent the movement of the IL droplet under the electric field gradient, a wall-like patterned positive-resist (AZ-5214E) was constructed and the small IL droplet was introduced inside the wall structure. In this study, we used solvated IL Cu^{2+} containing 2,5,8,11-tetraoxadodecane (G3: Triglyme) [23], [24]. It was obtained by mixing $Cu(Tf_2N)_2$ with G3 in a 1:1 molar ratio. The resulting equimolar complex of G3-$Cu(Tf_2N)_2$ was a liquid, and Cu^{2+} ion concentration was estimated to be 5.5 mol/L. The solvated IL allowed easy access of Cu^{2+} to the anode by forming the metal complex [24]. The device cross-section is shown in Fig. 1(a). The device's optical microscope image is shown in

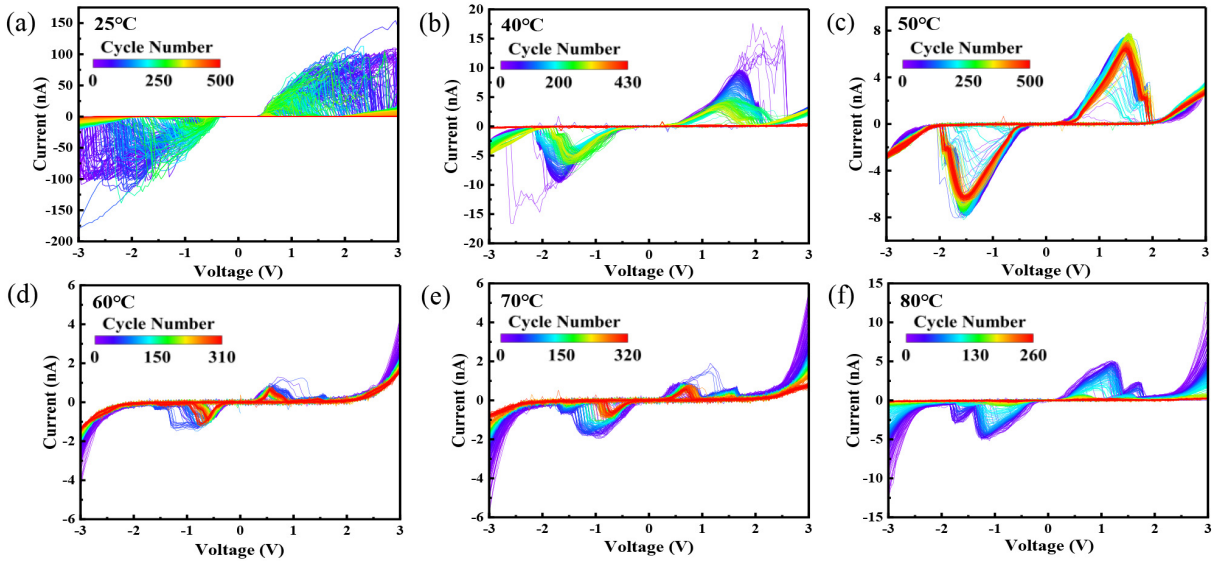

FIGURE 5. **(a)–(f) *I–V* characteristics at different temperatures.**

Fig. 1(b). The current–voltage (*I–V*) curves were measured at various temperatures using a semiconductor parameter analyzer (Agilent B1500A). The temperature and cycle speed dependence of the *I–V* characteristics of this device was evaluated. The sample-stage temperature was controlled to be at 25°C (room temperature), 40°C, 50°C, 60°C, 70°C, 80°C, 90°C, 100°C, and 120°C. After the sample-stage temperature reached the desired value, a 5-min waiting time was introduced for temperature stabilization. Optical microscopy was used to examine the device's reactive area after the *I–V* curve measurement.

In this study, we demonstrated the data classification using the measured current values. Because there were more than two classes in this case, temperature values during device operation, the error correcting output code (ECOC) model was adopted. Although a single IL-IConnect device was employed for the current measurement, a virtual node method can be used to obtain a high-dimensional input vector [25]. Every voltage application cycle yielded the dataset of 122 current values, equivalent to the 122-dimensional input vector. For each class label, 70 datasets were used for the learning process, while 30 datasets were used for the evaluation process. In the present study, the above-mentioned classification task was conducted using MATLAB (version R2021a, Mathworks).

III. RESULTS AND DISCUSSION

Fig. 2(a) shows the *I–V* curve measured at 25°C using the IL-IConnect device in its as-fabricated state. The voltage was first swept in the positive bias direction, and a gradual current increase was observed at around +2 V (sweep 1). Because the Cu cations were dissolved in the IL, the Cu reduction reaction on the grounded electrode occurred during voltage sweep, whereas the oxidation reaction on a positively biased counter electrode was possibly due to H_2O and O_2 in the IL.

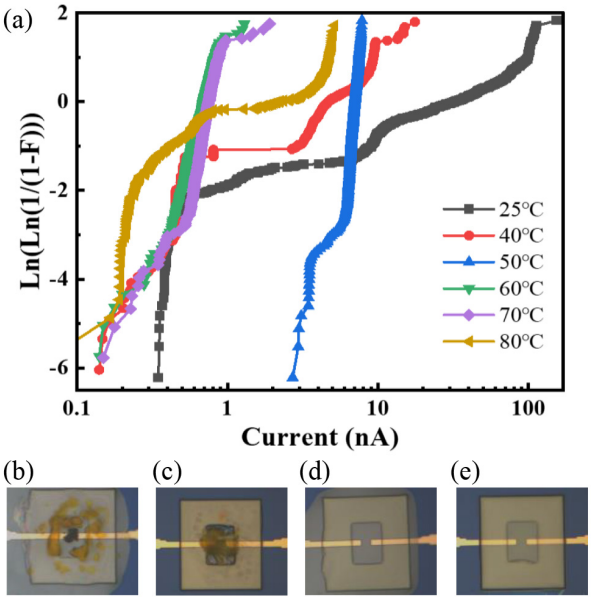

FIGURE 6. **(a) Weibull plot of peak current at different temperatures. (b)–(e) Microscopic observation images after cycle operations at 25°C, 40°C, 50°C, and 60°C, respectively.**

In the continuous sweep to the negative vias (sweep 2), a sharp peak appeared at approximately −0.5 V, attributable to both the Cu reduction and oxidation reactions. In this sweep, the current started increasing at a lower voltage than in the first voltage sweep because the observed current was primarily based on the reaction between the Cu metal and Cu cations. A subsequent rapid current decrease corresponded to the transition to the passive state due to the Cu oxide formation on the grounded electrode. The Cu oxide broke down and the current increased again when the external voltage was swept further to the negative bias. In sweep

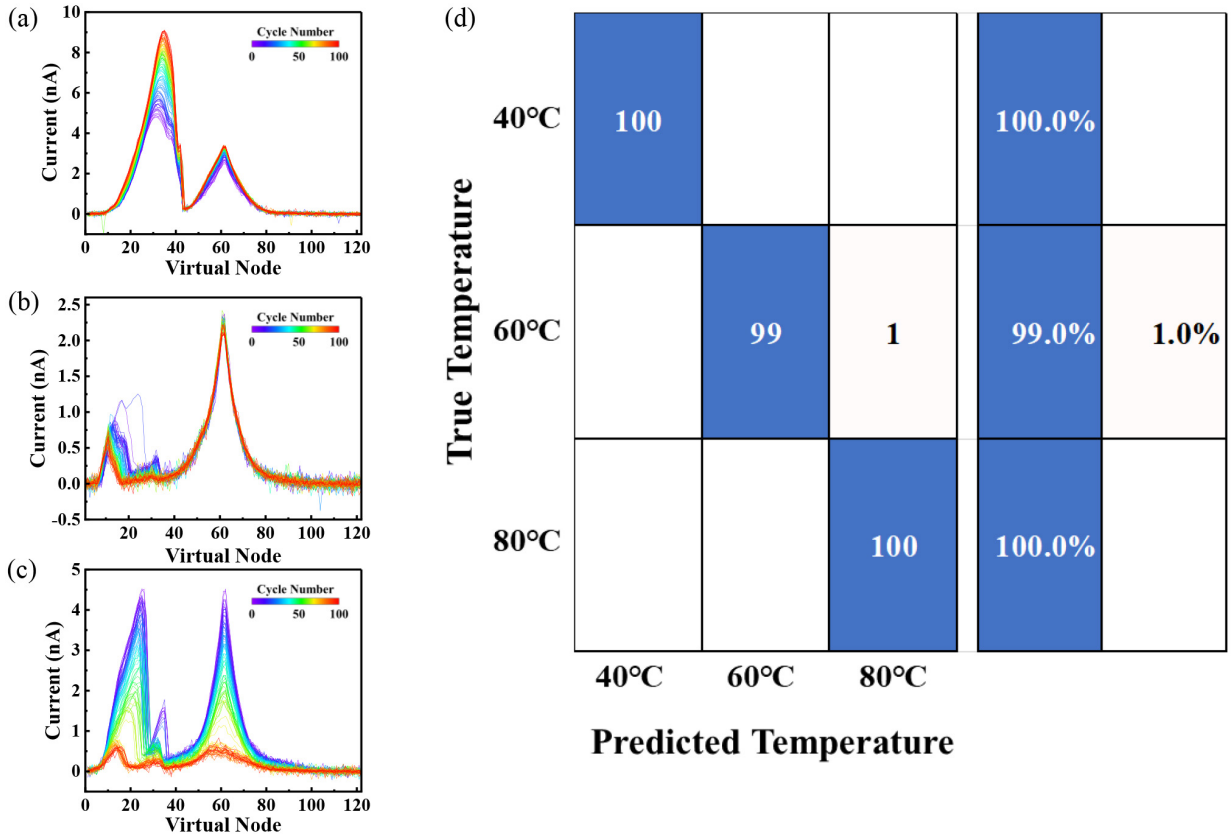

FIGURE 7. **(a)–(c) Current value of each temperature 40°C, 60°C, and 80°C are plotted by 122 virtual nodes, respectively, (d) classification results for *I–V* curves at three different temperatures.**

3 of Fig. 2(b), two current peaks were observed, and similar phenomena were observed at the Cu deposition/stripping processes on Pt(111) from Cu cations in 0.1 M H_2SO_4 [26]. When the IL contains no Cu ions, as reported in Ref. 27, the above-mentioned peaks of Faraday current will not be observed [27]. Fig. 3 shows the cycle dependence of the *I–V* curves at a 50 mV/sec sweep speed and 25°C temperature. The peak current decreased, and we observed yellow precipitates around the electrode by optical microscopy. Figs. 4(a) and 4(b) show the peak current tendency versus cycles at 50 and 600 mV/sec sweep speeds, respectively. At the 50 mV/sec, the peak current gradually decreases, and faded out around 30 cycles; however, the cycle repeatability increases dramatically at 600 mV/sec, From this result, we assessed *I–V* characteristics under different temperatures from 25°C to 80°C at 600 mV/sec. Figs. 5(a)–(f) show the results of *I–V* characteristics at 600 mV/sec and different temperatures. Despite the same input signal, the patterns of output signals are significantly different at 600 mV/sec with an increase in temperature. The patterns changed at 10°C, and clear cycles were accomplished at 50°C; this indicates that 50°C is the appropriate temperature at the 600mV/sec sweep speed, i.e., the reaction speed of Cu ion precipitation and dissolution on a Pt electrode is balanced and stable. Fig. 6(a) shows the result of the Weibull plot of peak current at different temperature conditions. The best linearity is obtained at 50°C. Meanwhile, *I–V* curves are distributed in a wide range of 25°C–40°C. This result indicates that a certain phenomenon occurred that prevented the redox reaction around the Pt electrode. We also performed microscopic observation during the *I–V* measurement (Fig. 6(b)–(e)). From the observation results, yellow precipitates formed below 40°C(Fig. 6(c)), and no precipitate was observed over 50°C (Fig. 6(d)), indicating that the dissolution reaction rate of yellow and Cu precipitates are slow below 40°C but balances at 50°C. In addition, above 60°C, the peak current around 1–2 V was smaller than the peak current value below 50°C, and no precipitation was observed around the Pt electrode by optical microscopy. From the results, temperature significantly influenced the electrochemical reaction in the metal ion solution IL. We also performed temperature recognition task experiments using a classifier trained by the support vector machine algorithm at 40°C, 60°C, and 80°C to confirm that the *I–V* curves have temperature information [28]. Figs. 7(a)–(c) depict the current value plotted at each virtual node. The virtual nodes are defined as a positive voltage range (0–3 V). Fig. 7(d) shows the classification results for *I–V* curves at three temperatures. Almost all output signals labeled at each temperature recognized the true temperature. It was thus found that the output signals of this device include surrounding temperature information, indicating that the IL-IConnect device can be used for

AI information processing in scenes that require different recognitions and judgments temperature-sensitive neuromorphic information processing device because inhibitory neurons in the human brain are activated at appropriate temperatures.

IV. CONCLUSION

In this study, we measured *I–V* sweep for an IL-IConnect device at different sweep speeds and temperatures. At the voltage sweep rate of 600 mV/sec and 50°C temperature, highly reliable cyclic voltammetry was observed. The experimental results show that the operating temperature range can be controlled by selecting a stable redox reactant in IL, indicating that the IL-IConnect device can act as a physical reservoir. The output signal of this device significantly depended on the temperature, and it changed despite applying the same signal. The results of this study clearly indicate that the IL-IConnect device has great potential applications in AI information processing and allows unique recognition and judgment including the temperature information. We believe that further investigation to optimize and improve the variation of ILs will enhance the device to produce novel reservoir properties for interconnects. The strong temperature dependence of the IL-IConnect device's operation can be useful for emerging devices, in which information processing senses temperature. From the IoT edge device application perspective, the devices are required to operate at relatively low power consumption. For the implementation of more advanced functions, the appropriate read-out interface for the ultralow operating current device, such as the present IL-IConnect device, is required, as reported in the literature [29], [30]. Further study to integrate the IL-IConnect device with the CMOS circuit will promote the implementation of the IL-IConnect device into the various scene to optimize the edge device operations based on the temperature information.

REFERENCES

[1] "International roadmap for devices and systems." IEEE. 2021. [Online] Available: https://irds.ieee.org/editions/2021
[2] M. Min and S. Kadivar, "Accelerating innovations in the new era of HPC, 5G and networking with advanced 3D packaging technologies," in *Proc. IWLPC*, San Jose, CA, USA, Oct. 2020, pp. 1–6, doi: 10.23919/IWLPC52010.2020.9375855.
[3] Y. S. Zou, C. L. Gan, M.-H. Chung, and H. Takiar, "A review of interconnect materials used in emerging memory device packaging: First- and second-level interconnect materials," *J. Mater Sci. Mater. Electron.*, vol. 32, pp. 27133–27147, Oct. 2021.
[4] B. D. Salvo, "Brain-inspired technologies: Towards chips that think?" in *Proc. ISSCC*, San Francisco, CA, USA, Feb. 2018, pp. 12–18, doi: 10.1109/ISSCC.2018.8310165.
[5] A. Nayak *et al.*, "Rate-limiting processes determining the switching time in a Ag_2S atomic switch," *J. Phys. Chem. Lett.*, vol. 1, no. 3, pp. 604–608, Jan. 2010.
[6] K. Gacem *et al.*, "Neuromorphic function learning with carbon nanotube based synapses," *Nanotechnology*, vol. 24, no. 38, pp. 1–9, Sep. 2013.
[7] H. Shima, M. Takahashi, Y. Naitoh, and H. Akinaga, "Electrode material dependence of resistance charge behavior in Ta_2O_5 resistive analog neuromorphic device," *IEEE J. Electron Devices Soc.*, vol. 6, pp. 1220–1226, 2018, doi: 10.1109/JEDS.2018.2875942.
[8] M.A. Akai-Kasaya *et al.*, "Evolving conductive polymer neural networks on wetware," *J. Appl. Phys.*, vol. 59, no. 6, May 2020, Art. no. 60601.
[9] D. Kim and J.-S. Lee, "Designing artificial sodium ion reservoirs to emulate biological synapses," *NPG Asia Mater*, vol. 12, p. 62, Sep. 2020.
[10] N. Banno *et al.*, "Three-fold improved set-voltage variability of a Cu atom switch with a split electrode for very-large-scale integration," *J. Appl. Phys.*, vol. 59, no. SG, pp. 237–245, Feb. 2020.
[11] M. Cucchi *et al.*, "Reservoir computing with biocompatible organic electrochemical networks for Brain-inspired biosignal classification," *Sci. Adv.*, vol. 7, no. 34, Aug. 2021, Art. no. ebh0693.
[12] R. Islam *et al.*, "Device and materials requirements for neuromorphic computing," *J. Phys. D, Appl. Phys.*, vol. 52, Jan. 2019, Art. no. 113001.
[13] J. H. Cha *et al.*, "Conductive-bridging random-access memories for emerging neuromorphic computing," *Nanoscale*, vol. 12, pp. 14339–14368, Apr. 2020.
[14] H. Sato *et al.*, "Memristors with controllable data volatility by loading metal ion-added ionic liquids," *Front. Nanotechnol.*, vol. 3, Mar. 2021, Art. no. 660563.
[15] G. Tanaka *et al.*, "Recent advances in physical reservoir computing: A review," *Neural Netw.*, vol. 115, pp. 100–123, Jul. 2019.
[16] R. Midya *et al.*, "Reservoir computing using diffusive Memristors," *Adv. Intell. Syst.*, vol. 1, no. 7, Sep. 2019, Art. no. 1900084.
[17] D. Sato *et al.*, "Development of physical reservoir devices utilized redox reactions of Cu and Ag ions in ionic liquids," presented at MEMRYSIS, Ibaraki, Japan, Nov. 2021.
[18] S. Caporali, P. Marcantelli, C. Chiappe, and C. S. Pomelli, "Electrodeposition of transition metals from highly concentrated solutions of ionic liquids," *Surface Coat. Technol.*, vol. 264, pp. 23–31, Feb. 2015.
[19] S. Kan, K. Nakajima, T. Asai, and M. Akai-Kasaya, "Physical implementation of reservoir computing through electrochemical reaction," *Adv. Sci.*, vol. 9, no. 6, Dec. 2021, Art. no. 2104076.
[20] W. Shao, Y. Sun, Y. Xu, and G. Zangari, "Depolarization of Cu electrodeposition in the presence of Ag: A cyclic-voltammetry study," *Electrochimica Acta*, vol. 405, Feb. 2022, Art. no. 139796.
[21] S. Kim *et al.*, "Neuronal dynamics in HfO_x/AlO_y-based homeothermic synaptic memristors with low-power and homogeneous resistive switching," *Nanoscale*, vol. 11, pp. 237–245, Nov. 2018.
[22] L. P. Buchwalter, "Chromium and tantalum adhesion to plasma-deposited silicon dioxide and silicon nitride," *J. Adhes Sci. Technol.*, vol. 9, no. 1, pp. 97–116, Jan. 2012.
[23] H. Yamaoka *et al.*, "Significantly improved performance of a conducting-bridge random access memory (CB-RAM) device using copper-containing glyme salt," *Chem. Lett.*, vol. 46, pp. 1832–1835, Oct. 2017.
[24] K. Yoshida *et al.*, "Oxidative-stability enhancement and charge transport mechanism in glyme-lithium salt equimolar complexes," *J. Am. Chem. Soc.*, vol. 133, pp. 13121–13129, Jul. 2011.
[25] L. Appeltant *et al.*, "Information processing using a single dynamical node as complex system," *Nat. Commun.*, vol. 2, pp. 1–6, Sep. 2011.
[26] M. Hayyan *et al.*, "Investigating the electrochemical windows of ionic liquids," *J. Ind. Eng. Chem.*, vol. 19, pp. 106–112, Jul. 2013.
[27] J. H. White and H. D. Abruña, "Influence of competing adsorbates on the underpotential deposition of copper on Pt(111)," *J. Electroanal. Chem. Interfacial Electrochem.*, vol. 300, pp. 521–542, Feb. 1991.
[28] C. Cortes and V. Vapnik, "Support-vector networks," *Mach. Learn.*, vol. 20, pp. 273–297, Mar. 1995.
[29] T. Yajima, "Ultra-low-power switching circuits based on a binary pattern generator with spiking neurons," *Sci. Rep.*, vol. 12, pp. 1–10, Jan. 2022.
[30] Y. Huang, F. Maloberti, and R. P. Martins, "Nano-ampere low-dropout regulator designs for IoT device," *IEEE Trans Circuit Syst. I, Reg. Papers*, vol. 65, no. 11, pp. 4017–4026, Nov. 2018, doi: 10.1109/TCSI.2018.2851226.